Optical Materials 120 (2021) 111457

Contents lists available at ScienceDirect

Optical Materials

journal homepage: www.elsevier.com/locate/optmat

Research Article

Evaluation on output parameters of the inverted organic solar cells depending on transition-metal-oxide based hole-transporting materials

Çağlar Çetinkaya [a,b], Erman Çokduygulular [c], Barış Kınacı [a,d,*], Feyza Güzelçimen [a], İdris Candan [e], Halil İbrahim Efkere [f,g], Yunus Özen [d,f], Süleyman Özçelik [d,h]

[a] Physics Department, Faculty of Science, Istanbul University, TR-34134, Istanbul, Turkey
[b] Graduate School of Engineering and Science, Istanbul University, TR-34116, Istanbul, Turkey
[c] Department of Engineering Sciences, Faculty of Engineering, Istanbul University-Cerrahpaşa, TR-34320, Istanbul, Turkey
[d] Photonics Application and Research Center, Gazi University, TR- 06500, Ankara, Turkey
[e] Department of Physics, Kocaeli University, TR-41001, İzmit, Kocaeli, Turkey
[f] Department of Physics, Faculty of Science, Gazi University, TR-06500, Ankara, Turkey
[g] Department of Metallurgical and Materials Engineering, Faculty of Technology, Gazi University, TR-06500, Ankara, Turkey
[h] Department of Photonics, Faculty of Applied Sciences, Gazi University, TR-06500, Ankara, Turkey

ARTICLE INFO

Keywords:
Organic solar cell
Transition-metal-oxide
Hole transport layer
P3HT:PCBM
UV–Vis–NIR spectroscopy
Atomic force microscopy
Power conversion efficiency

ABSTRACT

The study was focused on evaluating the effects of different hole transport layers (HTL) on optical, morphological, and electrical properties of organic solar cell (OSC) structures. Structuring the photoactive layer with blends of poly (3-hexylthiophene) (P3HT), and [6,6]-phenyl-C61-butyric acid methyl ester (PCBM) was practiced via spin coating technique. Transition-metal-oxides of vanadium pentoxide (V_2O_5), tungsten trioxide (WO_3), and molybdenum trioxide (MoO_3) as thin films with 10 nm thick were used for the HTL layers. The deposition of all interface layers except for P3HT:PCBM photoactive layer were radio-frequency (RF) magnetron sputtered. The surface morphological and optical properties of structures produced were examined by analyzing the UV–Vis–NIR and atomic force microscopy (AFM) measurements. The solar cell output parameters of the inverted OSCs produced were identified depending on transition-metal-oxide (TMO) based hole-transporting materials. MoO_3 HTL was exhibited as smoothest interface with a root mean square (RMS) surface roughness value of 7.11 nm. The power conversion efficiency (PCE) values of OSCs with HTL of V_2O_5, WO_3 and MoO_3 were found as 1.91%, 2.04% and 2.11%, respectively. With a comparative investigation was reported that an OSC structure with HTL of MoO_3 thin film providing optimal device performance in the present study might be preferred as an alternatively effective material for opto-electronic applications.

1. Introduction

Nowadays, scientific studies in polymer solar cells (PSCs) have advanced in power conversion efficiency (PCE) for both single- and multi-junction devices [1–6]. It is noteworthy that PSCs can be applied in both conventional and inverted device architectures. The inverted ones, which are widely used, exhibit with long-term stability and light-harvesting capability. Over the past twenty years, the bulk heterojunction (BHJ) based PSCs have been the focused subject of a swiftly developing area. Their potential role in SCs and inflexible devices as an alternative semiconductor material due to their unique advantages like easy fabrication, low-cost solution-based processing have been investigated [7–9]. Organic semiconductor materials based on hydrocarbon molecules are one of the promising candidates as an alternate material. Therefore, the underlying science of organic solar cells (OSCs) based on conjugated polymers have led to advances since the exploration of effective photo-induced charge carrier segregation at donor-acceptor interfaces [7,9]. Additionally, the materials used in OSCs have flexible atomic structures that can be easily produced, lightweight, non-toxic, color adjustable absorbent materials occurred abundantly in nature.

For tuning the HOMO and LUMO levels of BHJ based photoactive layer and the top and bottom metal electrodes in the OSCs, two different metal oxide layers are individually used as an electron transport layer (ETL) and a hole transport layer (HTL). So that the charge carriers drifting towards the electrodes in the structure do not meet a serious potential barrier and ohmic contact properties are obtained in the SC.

* Corresponding author. Physics Department, Faculty of Science, Istanbul University, TR-34134, Istanbul, Turkey.
E-mail address: baris.kinaci@istanbul.edu.tr (B. Kınacı).

https://doi.org/10.1016/j.optmat.2021.111457
Received 21 June 2021; Received in revised form 26 July 2021; Accepted 4 August 2021
Available online 10 August 2021
0925-3467/© 2021 Elsevier B.V. All rights reserved.

Moreover, these metal oxide layers act as an optical separator that localizes the distribution of incoming light in the center and around the photoactive layer to achieve maximum short circuit current in OSCs. An inverted structure of transparent electrodes/ETL/photoactive layer/HTL/top metal electrodes is more commonly used in both flexible and ultrathin OSCs because the conventional structure of OSCs is directly affected by the imperfect gas barrier property of substrates and passivation layers. Additionally, the inverted structure of OSCs is more suitable for stability in the long term [10,11].

In inverted OSC (IOSC), the ETL with a low work function is placed in between the photoactive layer and the ITO or FTO bottom contact, thereby changing the interface and enhancing the transport of electrons separated from the photoactive layer. However, the presence of metal contact with a high work function directly on the photoactive layer adversely affects the performance of the IOSCs. Therefore, HTL should be added between the photoactive layer and metal contact to efficiently collect the holes and block electrons. To get good performance from an IOSC, the device will perform poorly or not at all if an HTL layer is not added between the organic active layer and the top metal electrode [12].

A transition-metal-oxide (TMO), such as MoO_3, V_2O_5, WO_3, SnO_2 and Co_3O_4, etc. having air stability and high optical transparency, insolubility in some solvents, or organic materials treated with PEDOT:PSS, SPDPA, and PCDTBT are given priority as an efficient HTL for stable OSCs [13–21].

It is well-known that MoO_3 has prominent consideration with higher solar cell performance due to relatively good hole-mobility and transparency [22]. There are already studies on using MoO_3 as HTL in P3HT:PCBM-based IOSCs [16,19,23–25]. In these studies, we noticed that the thermal evaporation system was particularly carried out as the deposition system and the thickness of MoO_3 as a HTL structure varied in the range of 1–15 nm. The studies exhibited that the V_{oc} and *FF* values varied in the range from 0.50 V to 0.658 V and from 44% to 62.3%, respectively. In addition, Wantz et al. presented that the performance of a P3HT:PCBM-based device was weakly influenced with a change of the MoO_3 thickness from 6 to 22 nm [26].

WO_3 efficiently extracts holes and suppresses electrons from the active layer due to the high work function, so it can efficiently act as a HTL [22]. The studies examining WO_3 used as HTL in P3HT:PCBM-based IOSCs exist in the literature [20,27]. By thermal evaporation system selected as the deposition system in these studies, it was reported that the optimum thickness of WO_3 used as HTL in P3HT:PCBM-based IOSCs was in the range of 5–10 nm [12,20]. The studies represented that the V_{oc} and *FF* values were between 0.597 V and 0.600 V, and between 59% and 60%, respectively.

Having a band-gap of 2.42 eV, a low electron affinity of 2.94 eV and ionization energy around 5.36 eV, which indicate that V_2O_5 can form an efficient HTL in an OSC device [22]. Although it has been commonly used as HTL in inverted devices, it can not be a suitable structure for devices with low-cost and easy-to-produce in ambient conditions due to its high toxicity [28]. Nevertheless, V_2O_5 as HTL in P3HT:PCBM-based IOSCs has also been the subject in the literature [15,29,30]. In particular, the spin coating and thermal evaporation systems were performed as deposition system and the evaluations of results depended on a basis of V_2O_5 concentration. As seen in these studies, the output parameters of V_{oc} and *FF* changed from 0.530 V to 0.563 V, and from 47.20% to 60.21%, respectively.

For similar structures in the literature, different OSC output parameters were obtained by various deposition techniques and under different conditions [15–20, 23–32]. It is clear that the variation of deposition technique, deposition conditions as well as layer thicknesses of devices dramatically affect the output parameters of the OSC. Therefore, the comparison between the results for unsame structures can be considered as not relative. It is quite significant to produce HTLs under the same conditions so that the cell output parameters to be obtained in the studies are metrologically reproducible and comparable. As far as we know from the literature, there is no recently current research paper (except reviews) presenting the relatively comparison of the effect of HTL structures, which is the main focus of this study, under the same deposition conditions in sputtering technique. Therefore, our study includes metrologically reproducible and comparable measurement results.

We have preferred the sputtering technique, which has better repeatability and controllability of parameters such as vacuum chamber pressure, substrate temperature, deposition rate, deposition time and substrate rotation. In addition, the MoO_3, V_2O_5, WO_3 targets (with a purity of 99.99%) compounds used in the sputter system enable us precisely determine the accurate elemental composition and atomic stoichiometry of TMO structures deposited on polymer [33]. In particular, metal oxides such as MoO_3, WO_3 and V_2O_5 that can be evaporated at relatively mild temperatures have suitable utilization for devices produced in a vacuum environment [34].

Here we have reported the effects of MoO_3, V_2O_5, and WO_3 TMOs as HTL on the solar cell parameters of the BHJ-based IOSCs. These HTLs were deposited between the anode metal contact and the P3HT:PCBM active layer of IOSCs by RF sputtering system. The transmittance $T(\lambda)$ spectra and surface morphologies of Glass/FTO/ZnO/P3HT:PCBM/HTL (MoO_3, V_2O_5 or WO_3) structures were evaluated by performing UV–Vis–NIR spectroscopy and atomic force microscopy (AFM) systems. In addition, the I-V measurements were carried out under 1.5 a.m. irradiation in order to obtain SC device parameters of inverted Glass/FTO/ZnO/P3HT:PCBM/HTL (MoO_3, V_2O_5 or WO_3)/Ag OSCs. In particular, the power conversion efficiency (PCE) values of devices produced were compared to each other.

2. Material and method

In the photoactive region, the blend of the poly (3-hexylthiophene) (P3HT) as a donor, and [6,6]-phenyl-C61-butyric acid methyl ester (PCBM) as an acceptor was practiced for all the OSCs devices. The layer thicknesses, except HTL, of devices in this study were produced by keeping in the same values. The deposition of P3HT:PCBM photoactive region was provided with a spin coater system. By applying a RF sputtering system (Nanovak NVTS500), all other layers of OSC devices were fabricated. Schematic illustration of inverted OSC device structures is shown in Fig. 1.

Fluorine tin oxide (FTO) coated glass substrates are extensively used as a bottom electrode due to their high optical transmittance of approximately 90% and low operating function of about 4.4 eV as well as electrically conductive. Before device production, all samples of FTO-coated glass substrates were cleaned to remove organic and inorganic contaminants. In the cleaning process, the substrates were ultrasonically washed by immersing in a detergent solution and deionized water for 5 min, and then rinsed with distilled water. After an ultrasonic bath in different containers with pure acetone and isopropyl alcohol was used to clean the samples up to 10 min, the samples were dried with high-purity nitrogen gas (N_2).

ZnO thin film layer, with a total thickness of ~40 nm, acted as ETL was deposited onto the samples by RF sputtering technique from a ZnO target of 99.999% purity. P3HT and PCBM were commercially purchased from Sigma-Aldrich and dissolved with wt-ratio of 1:1 in Dichlorobenzene (DCB) solvent by means of a magnetic stirrer at temperature of 40 °C for 14 h. The solution of P3HT:PCBM blend was coated onto Glass/FTO/ZnO structures with 600 rpm for 20 s and fallowed with 1100 rpm for 9 s via Süss Microtec 6 RC spin coater system at room temperature. As a post-production process, heat treatment was applied to Glass/FTO/ZnO/P3HT:PCBM on a hot plate at 150 °C for 5 min in order to disperse the solvents remained in the structure and to improve the photoactive layer.

Each TMO layer followed by the thickness of 10 nm were separately coated onto Glass/FTO/ZnO/P3HT:PCBM structures by RF sputtering system using with high-purity (99.999%) MoO_3, WO_3, and V_2O_5 targets. Then, the metal contact of Ag was deposited on top of all Glass/FTO/

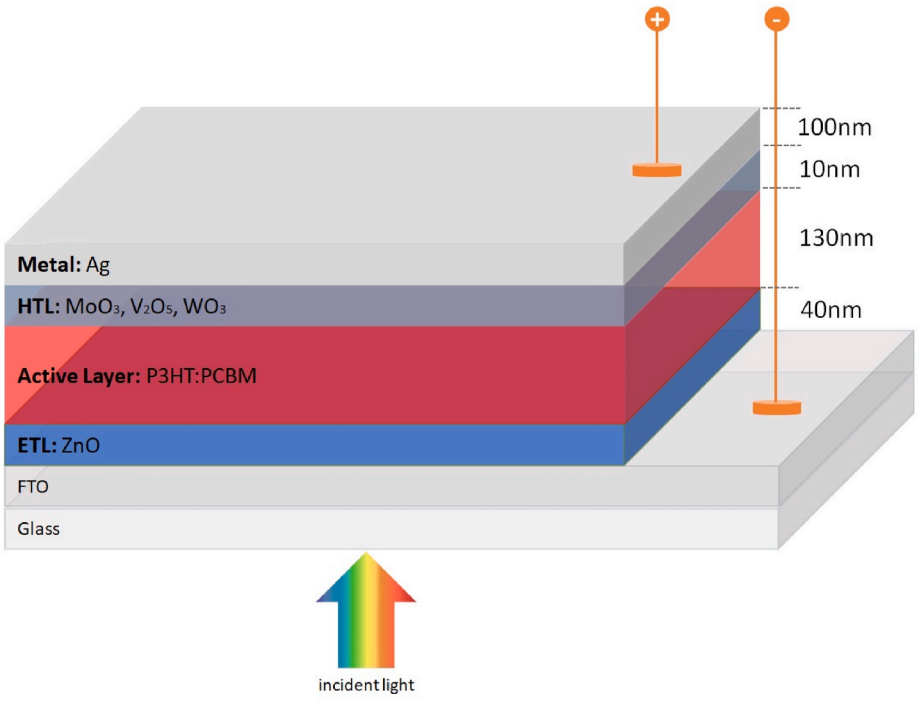


Fig. 1. Schematic illustration of inverted OSC device structures.

ZnO/P3HT:PCBM/HTL structures by RF sputtering system from Ag target of 99.999% purity. The layer thicknesses and labeling of structures produced with and without HTL layer are presented in Table 1.

Transmittance spectra of structures labelled with GFZ, GFZPM, GFZPV, and GFZPW were recorded with a PerkinElmer Lambda 2S UV–Vis–NIR spectrometer in the wavelength range of 200 − 1100 nm in order to study on optical characteristics. Surface morphological images over a scanning area of 5×5 μm^2 at room temperature conditions were monitored with high-performance AFM system (hpAFM) (Nano-Magnetics Instruments LTD., Oxford, UK). We investigated the performance of OSC devices based on different TMO layers. In this framework, we used the Keithley 4200 source meter the current density-voltage ($J-V$) measurements and the Newport Oriel-Sol1A solar simulator for AM 1.5G illumination.

3. Results and discussion

3.1. Surface morphological and electrical analyses of OSC structure without HTL

By performing AFM to monitor the surface morphology of P3HT:PCBM active layer on ZnO (Fig. 2), the root mean square (RMS) surface roughness value was measured as 3.13 nm.

Table 1
The layer thicknesses and labeling of the structures produced.

Structure	Layer thicknesses	Labeling
Glass/FTO/ZnO	−/−/40 nm	GFZ
Glass/FTO/ZnO/P3HT:PCBM	−/−/40nm/130 nm	GFZP
Glass/FTO/ZnO/P3HT:PCBM/V_2O_5	−/−/40nm/130nm/10 nm	GFZPV
Glass/FTO/ZnO/P3HT:PCBM/WO_3	−/−/40nm/130nm/10 nm	GFZPW
Glass/FTO/ZnO/P3HT:PCBM/MO_3	−/−/40nm/130nm/10 nm	GFZPM
Glass/FTO/ZnO/P3HT:PCBM/Ag	−/−/40nm/130nm/100 nm	GFZPA
Glass/FTO/ZnO/P3HT:PCBM/V_2O_5/Ag	−/−/40nm/130nm/10nm/100 nm	GFZPVA
Glass/FTO/ZnO/P3HT:PCBM/WO_3/Ag	−/−/40nm/130nm/10nm/100 nm	GFZPWA
Glass/FTO/ZnO/P3HT:PCBM/MO_3/Ag	−/−/40nm/130nm/10nm/100 nm	GFZPMA

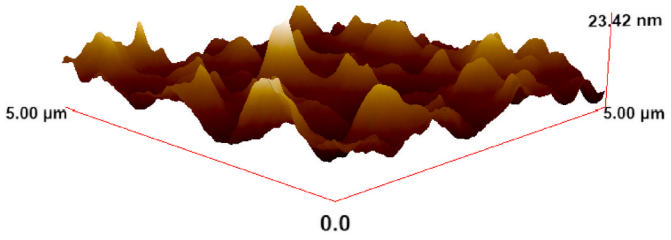


Fig. 2. AFM image of the 3D configuration of P3HT:PCBM on ZnO.

The electrical analysis of GFZPA as the reference sample without TMO layer was carried out with the determination of current density-voltage ($J-V$) and power-voltage ($P-V$) characteristics at room tem-

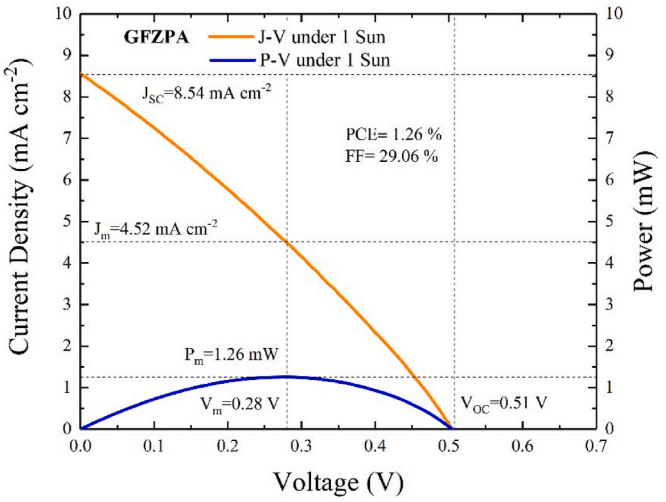


Fig. 3. The current density-voltage ($J-V$) and power-voltage ($P-V$) characteristics of GFZPA.

perature conditions. As illustrated Fig. 3, the maximum values of current density (J_m), voltage (V_m), power (P_m) as well as the SC parameters of open-circuit voltage (V_{oc}), short-circuit current density (J_{sc}), fill factor (*FF*) and *PCE* for GFZPA sample were found as 4.52 mA cm^{-2}, 0.28 V, 1.26 mW, 0.51 V, 8.54 mA cm^{-2}, 29.06%, and 1.26%, respectively.

3.2. Surface morphological, optical and electrical analyses of OSC structures with HTL

By examining the effect of HTL on cell output parameters, we have taken into consideration that the examination of the surface morphology between the active layer and the upper contact is quite significant. In support of this view, there are already studies in the literatüre [15,28]. Therefore, we have been emphasized the morphology of HTLs, under the top contact Ag, resulting of overlapping of each layer in the structures deposited layer by layer, instead of the investigation of the morphology of single layers (e.g. certain films).

We investigated the surface morphology of HTL based on TMO of MoO_3, WO_3, and V_2O_5 on P3HT:PCBM active layer. Three-dimensional (3D) topographic visualizations are gathered in Fig. 4. It has been pointed out that the representative RMS values of the V_2O_5, WO_3, and MoO_3 on P3HT:PCBM active layer were measured as 9.98 nm, 7.72 nm and 7.11 nm, respectively.

It is known that TMO deposited by the sputtering technique on the P3HT:PCBM active layer directly affects the surface morphology and considerably increases the RMS values [31]. In the sputtering technique, as energetic atoms from the compound target (with high-purity) arrived to the polymer surface, it is quite possible that atoms penetrate the microstructure of the polymer, transfer their energy to the P3HT:PCBM active layer as well as form surface defects. So, they can dramatically change the surface morphology in vacuum conditions [15,31].

The experimental results of cell electric output parameters indicate that the GFZPM device exhibits higher PCE than the other investigated ones. It is fact that a smoother surface commonly presents a trend as reducing both leakage current and contact resistance. It is well-known that the surface defects etc., which cause leakage current and contact resistance, encountered by the photo-generated carriers while being swept to the contacts directly affect the performance of the device [28, 32,35]. A smoother HTL surface is one of the properties that can enhance cell output parameters. Thus, it is considered that the GFZPMA structure can exhibit a better PCE value than the others.

The measurements of optical transmittance for GFZ, GFZPM, GFZPV and GFZPW structures labelled in Table 1 were recorded in the spectral region of 200 − 1100 nm at room temperature (Fig. 5). It is distinctly obvious as viewed from the spectra that the transparency of the samples exhibits a decrease in the range of 300 − 600 nm. Indeed, the spectra reveal that all samples presented high transmittance over the wavelength of 600 nm as expected.

The calculation of J_{ph} provides a prediction especially for J_{sc}, one of the cell output parameters of OSC, from the experimentally obtained optical characteristics. This is a commonly used and effective method to show whether the optical properties experimentally obtained are compatible with the electrical characteristics. The procedure also allows an estimation of relative photo-generated carriers for OSCs containing different HTLs. Therefore, J_{ph} values have been calculated based on the optical results in order to verify our experimental ones.

For the confirmation of the effect of HTL structure on electrical parameters, theoretical photocurrent density J_{ph} values were calculated in the entire wavelength range of the AM 1.5G spectral irradiance. The J_{ph} is:

$$J_{ph} = \int_{\lambda_{low}}^{\lambda_{up}} AM1.5G(\lambda)\, T(\lambda)\, \left(1 - e^{-\alpha(\lambda) d_{al}}\right) d\lambda \quad (1)$$

where $\alpha(\lambda)$ and d_{al} are the absorption coefficient and thickness of P3HT:PCBM, respectively.

Equation (1) is widely used for the determination of J_{ph}, taking into account the AM1.5G spectral irradiance and the transmittance characteristics of the GFZPV, GFZPW and GFZPM to be compared. J_{ph} values, which are calculated by using the experimental transmittance spectra for the OSC structures, are presented in Table 2.

The relative evaluation of photocurrent density was exhibited by considering the characteristic of AM1.5G in different wavelength ranges and variation of the absorption coefficient of the active region depending on wavelength. Because metal-oxide alloys, which take place

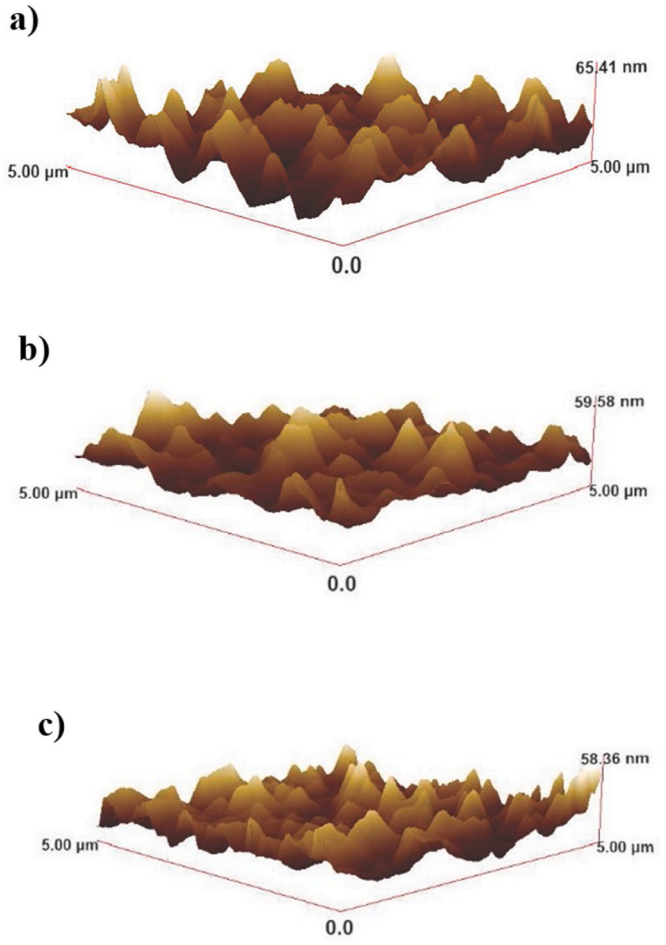


Fig. 4. AFM images of the 3D configuration of **a)** V_2O_5, **b)** WO_3, and **c)** MoO_3 on P3HT:PCBM active layer.

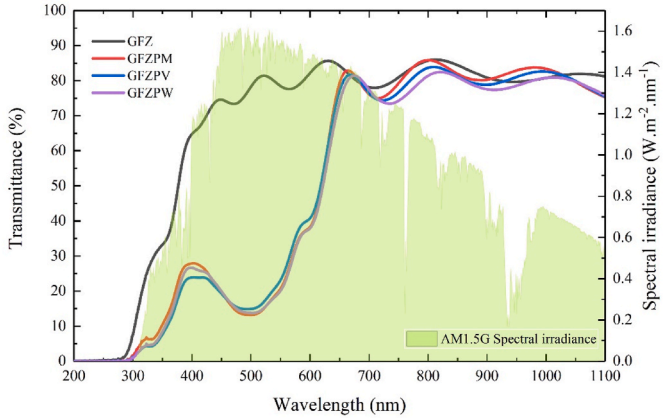


Fig. 5. Transmittance spectra for the GZF, GFZPM, GFZPV, and GFZPW.

Table 2
Calculated J_{ph} values of GFZPV, GFZPW and GFZPM.

OSC	GFZPV	GFZPW	GFZPM
J_{ph} $(mA \cdot cm^{-2})$	74.46	71.69	73.04

as HTL of GFZPM, GFZPV and GFZPW structures, have high transmittance and almost no absorbance, especially in the visible region [22,32,36–40]. Therefore, it should be noted here that the absorption characteristics of the structures are determined by the change of the absorption coefficient of the active region.

The transmittance of GFZPM is much higher than the other devices in the wavelength range of 300–450 nm (Fig. 6). However, since P3HT:PCBM absorption and AM1.5G spectral irradiance are low in this region, the highest J_{ph} does not belong to this structure. As resulting from AM1.5G spectral irradiance in the 450–600 nm range and P3HT:PCBM absorption in the 450–500 nm range are effectively high, it is of significance to examine the transmittance spectra of solar cells in these regions. From 450 to 600 nm, it is obviously indicated that the transmittance of GFZPV associated with the highest J_{ph} value is slightly higher than other structures produced.

Based on the main purpose of this study; in order to determine the effects of HTL structure in IOSC devices on solar cell output parameters, the device behaviors were examined for structures with and without HTL, which were deposited on FTO coated-glass used as the substrate, under the same vacuum conditions. The device structure of GFZPA without HTL was used as a reference one for the comparison to be made between the results. Fig. 7 represents current density-voltage ($J-V$) and power-voltage ($P-V$) characteristics of the devices with TMO layer at room temperature conditions. The J_{sc} values for the GFZPVA, GFZPWA, and GFZPMA structures are 8.11, 5.92 and 6.78 mA cm^{-2}, respectively. It is linked that these results are in a good agreement with the J_{ph} values as seen in Table 2.

The corresponding performance parameters based $J-V$ curves for the GFZPVA, GFZPWA, and GFZPMA devices are comparatively summarized in Fig. 8, which is demonstrated a comprehensive comparison the effects of HTL structure on the performance of OSCs. Among the TMOs used as HTL in OSCs, MoO_3 should be attracted prominent consideration giving the highest solar cell performance due to its relatively good hole mobility and transparency [22]. The experimental results of cell electric output parameters indicate that the GFZPMA device exhibits a better *PCE* than the other investigated devices with HTL/TMO. Thus, it can be confirmed that the OSC structure with MoO_3 HTL has optimal device performance parameters, since the in good

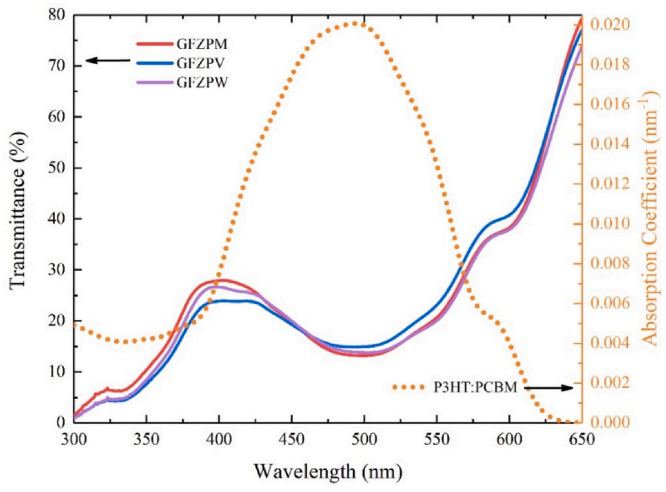


Fig. 6. Transmittance spectra for OSCs produced and absorption coefficient of P3HT:PCBM polymer depending on the wavelength range of 300–650 nm.

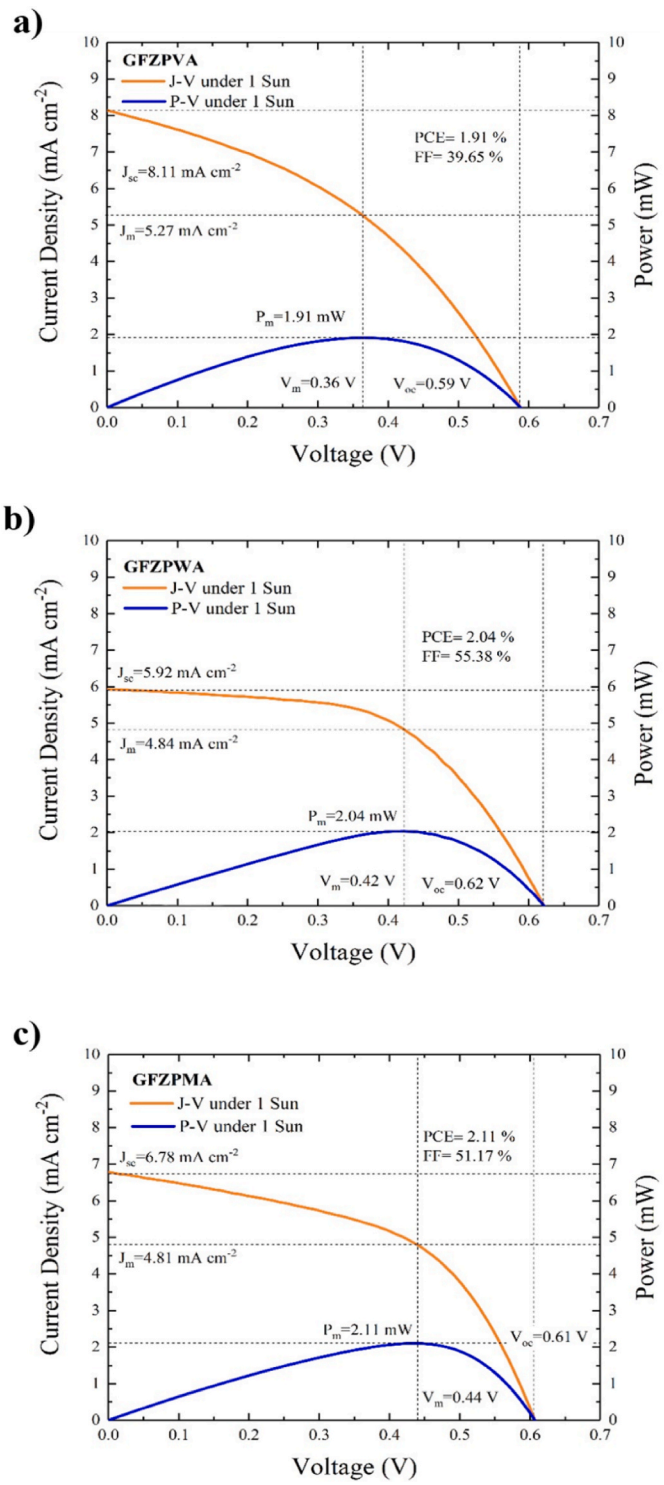


Fig. 7. The current density-voltage ($J-V$) and power-voltage ($P-V$) characteristics of devices with HTL/TMO; a) GFZPVA, b) GZPWA, and c) GFZPMA, at room temperature conditions.

agreement with results obtained by AFM and electrical measurements.

When we make an overall evaluation and comparison with the studies on similar OSC structures, which were produced under various deposition techniques and conditions as follows:

- The J_{sc} value ranged from 3.30 to 11.34 mA cm^{-2} in P3HT:PCBM based OSCs where MoO_3 was used as HTL [16,19,23–25] and was of 6.78 mA cm^{-2} for GFZPMA in our study. In addition, PCE values of

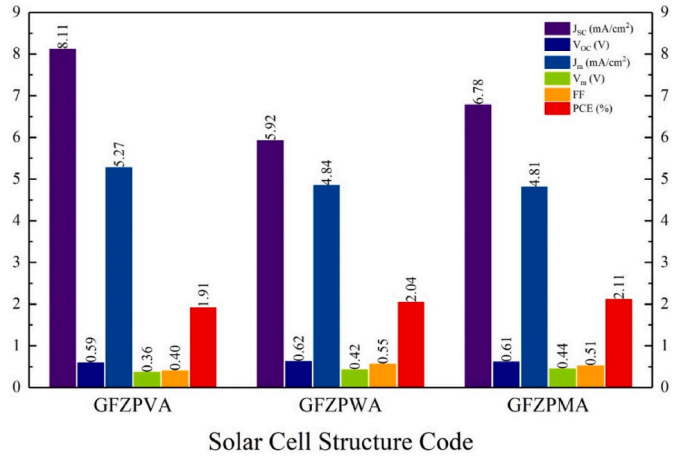


Fig. 8. Comparable OSC output parameters of GFZPVA, GFZPWA, and GFZPMA devices.

these OSCs were in the range of 0.96–3.78%, and in our study, this value was of 2.11% for GFZPMA.

- The J_{sc} value ranged from 5.40 to 7.20 mA cm^{-2} in P3HT:PCBM based OSCs where WO_3 was used as HTL [20,27] and was of 5.92 mA cm^{-2} for GFZPWA in our study. In addition, PCE values of these OSCs were in the range of 1.90–2.58%, and in our study, this value was of 2.04% for GFZPWA.
- The J_{sc} value ranged from 9.54 to 10.80 mA cm^{-2} in P3HT:PCBM based OSCs where V_2O_5 was used as HTL [15,29,30] and was of 8.11 mA cm^{-2} for GFZPVA in our study. In addition, PCE values of these OSCs were in the range of 2.58–3.56%, and in our study, this value was of 1.91% for GFZPVA.

Depending on parameters, which affect the cell performance, such as deposition technique, deposition conditions, layer thicknesses, etc., it is possible that the results obtained for the structures investigated may highly differ. Since the aim of the current study is to examine the effect of HTLs produced under the same deposition technique and same deposition conditions on cell performance, the relative comparison of the output parameters of GFZPMA, GFZPWA, and GFZPVA provides a more effective evaluation.

As we take a closer look at our results, it can be considered that the device performance of OSCs are apparently separated at their HTL interfaces. An evaluation combined with analysis of results revealed that an OSC structure with MoO_3 HTL might be used as an alternative material for interface layer to the OSC applications.

4. Conclusion

In summary, the effects of MoO_3, V_2O_5, and WO_3 TMOs as HTL on the SC parameters of the BHJ-based IOSCs were comparatively investigated. An RF sputtering system was applied to deposit of all layers except from P3HT:PCBM photoactive layer, which was coated with spin coating technique. By carrying out AFM technique in OSC structures without and with HTL, the values of RMS surface roughness were measured. UV–Vis–NIR spectroscopic techniques were performed to OSCs with HTL produced, and then the J_{ph} values were computed using the obtained experimental data. In the process of electrical experiments, the $J-V$ and $P-V$ characteristics at room temperature conditions were carried out for devices with HTL.

The sample with HTL of MoO_3 has dominated the smoothest interface with RMS value of 7.11 nm. The optimal device performance and high efficiency are achievable for OSC device of GFZPMA with a maximum efficiency of 2.11%, V_{oc} of 0.61 V, *FF* of 51.17% and J_{sc} of 6.78 mA cm^{-2}. As we take a closer look at our results, it can be considered that the device performance of OSCs are apparently separated at their HTL interfaces. An evaluation combined with analysis of results revealed that an OSC structure with MoO_3 HTL might be used as an alternative material for interface layer to the OSC applications.

In the light of the findings in the present study, various morphological, optical and electrical experiments of an OSC depending on all physical parameters of interfaces are deserved continuous investigation, as a better understanding of cell behavior.

CRediT authorship contribution statement

Çağlar Çetinkaya: Conceptualization, Formal analysis. **Erman Çokduygulular:** Formal analysis, Visualization. **Barış Kınacı:** Conceptualization, Writing – original draft. **Feyza Güzelçimen:** Visualization, Writing – review & editing. **İdris Candan:** Investigation, Writing – original draft. **Halil İbrahim Efkere:** Investigation. **Yunus Özen:** Resources. **Süleyman Özçelik:** Supervision.

Declaration of competing interest

The authors declare that they have no known competing financial interests or personal relationships that could have appeared to influence the work reported in this paper.

Acknowledgements

This work was supported by Gazi University Scientific Research Project Coordination Unit with project no: 05/2020-05 and the Directorate of Presidential Strategy and Budget of Turkey (Project No: 2019K12-149045).

References

[1] J. Yuan, Y. Zhang, L. Zhou, G. Zhang, H.-L. Yip, T.-K. Lau, X. Lu, C. Zhu, H. Peng, P. A. Johnson, M. Leclerc, Y. Cao, J. Ulanski, Y. Li, Y. Zou, Single-junction organic solar cell with over 15% efficiency using fused-ring acceptor with electron-deficient core, Joule 3 (2019) 1140–1151, https://doi.org/10.1016/j.joule.2019.01.004.

[2] Y. Cui, H. Yao, J. Zhang, T. Zhang, Y. Wang, L. Hong, K. Xian, B. Xu, S. Zhang, J. Peng, Z. Wei, F. Gao, J. Hou, Over 16% efficiency organic photovoltaic cells enabled by a chlorinated acceptor with increased open-circuit voltages, Nat. Commun. 10 (2019) 2515, https://doi.org/10.1038/s41467-019-10351-5.

[3] B. Fan, D. Zhang, M. Li, W. Zhong, Z. Zeng, L. Ying, F. Huang, Y. Cao, Achieving over 16% efficiency for single-junction organic solar cells, Sci. China Chem. 62 (2019) 746–752, https://doi.org/10.1007/s11426-019-9457-5.

[4] S. Liu, J. Yuan, W. Deng, M. Luo, Y. Xie, Q. Liang, Y. Zou, Z. He, H. Wu, Y. Cao, High-efficiency organic solar cells with low non-radiative recombination loss and low energetic disorder, Nat. Photonics 14 (2020) 300–305, https://doi.org/10.1038/s41566-019-0573-5.

[5] L. Meng, Y. Zhang, X. Wan, C. Li, X. Zhang, Y. Wang, X. Ke, Z. Xiao, L. Ding, R. Xia, H.-L. Yip, Y. Cao, Y. Chen, Organic and solution-processed tandem solar cells with 17.3% efficiency, Science 361 (80) (2018) 1094–1098, https://doi.org/10.1126/science.aat2612.

[6] J. Zhang, L. Zhu, Z. Wei, Toward over 15% power conversion efficiency for organic solar cells: current status and perspectives, Small Methods 1 (2017), 1700258, https://doi.org/10.1002/smtd.201700258.

[7] G. Yu, J. Gao, J.C. Hummelen, F. Wudl, a.J. Heeger, Polymer photovoltaic Cells : enhanced efficiencies via a network of internal donor-acceptor heterojunctions, Science 270 (80) (1995) 1789–1791, https://doi.org/10.1126/science.270.5243.1789.

[8] W. Ma, C. Yang, X. Gong, K. Lee, A.J. Heeger, Thermally stable, efficient polymer solar cells with nanoscale control of the interpenetrating network morphology, Adv. Funct. Mater. 15 (2005) 1617–1622, https://doi.org/10.1002/adfm.200500211.

[9] N.S. Sariciftci, L. Smilowitz, A.J. Heeger, F. Wudl, Photoinduced electron transfer from a conducting polymer to buckminsterfullerene, Science 258 (80) (1992) 1474–1476, https://doi.org/10.1126/science.258.5087.1474.

[10] K. Fukuda, K. Yu, T. Someya, The future of flexible organic solar cells, Adv. Energy Mater. 10 (2020), 2000765, https://doi.org/10.1002/aenm.202000765.

[11] P. Cheng, X. Zhan, Stability of organic solar cells: challenges and strategies, Chem. Soc. Rev. 45 (2016) 2544–2582, https://doi.org/10.1039/C5CS00593K.

[12] S. Lattante, Electron and hole transport layers: their use in inverted bulk heterojunction polymer solar cells, Electronics 3 (2014) 132–164, https://doi.org/10.3390/electronics3010132.

[13] C. Waldauf, M. Morana, P. Denk, P. Schilinsky, K. Coakley, S.A. Choulis, C. J. Brabec, Highly efficient inverted organic photovoltaics using solution based

titanium oxide as electron selective contact, Appl. Phys. Lett. 89 (2006) 1–4, https://doi.org/10.1063/1.2402890.
[14] M.Y. Chan, C.S. Lee, S.L. Lai, M.K. Fung, F.L. Wong, H.Y. Sun, K.M. Lau, S.T. Lee, Efficient organic photovoltaic devices using a combination of exciton blocking layer and anodic buffer layer, J. Appl. Phys. 100 (2006), https://doi.org/10.1063/1.2363649.
[15] J.-S. Huang, C.-Y. Chou, M.-Y. Liu, K.-H. Tsai, W.-H. Lin, C.-F. Lin, Solution-processed vanadium oxide as an anode interlayer for inverted polymer solar cells hybridized with ZnO nanorods, Org. Electron. 10 (2009) 1060–1065.
[16] A.K.K. Kyaw, X.W. Sun, C.Y. Jiang, G.Q. Lo, D.W. Zhao, D.L. Kwong, An inverted organic solar cell employing a sol-gel derived ZnO electron selective layer and thermal evaporated MoO_3 hole selective layer, Appl. Phys. Lett. 93 (2008), 221107, https://doi.org/10.1063/1.3039076.
[17] G. Li, C.W. Chu, V. Shrotriya, J. Huang, Y. Yang, Efficient inverted polymer solar cells, Appl. Phys. Lett. 88 (2006) 1–4, https://doi.org/10.1063/1.2212270.
[18] Y. Sun, J.H. Seo, C.J. Takacs, J. Seifter, A.J. Heeger, Inverted polymer solar cells integrated with a low-temperature-annealed sol-gel-derived ZnO film as an electron transport layer, Adv. Mater. 23 (2011) 1679–1683, https://doi.org/10.1002/adma.201004301.
[19] C. Tao, S. Ruan, X. Zhang, G. Xie, L. Shen, X. Kong, W. Dong, C. Liu, W. Chen, Performance improvement of inverted polymer solar cells with different top electrodes by introducing a MoO_3 buffer layer, Appl. Phys. Lett. 93 (2008) 2006–2009, https://doi.org/10.1063/1.3026741.
[20] C. Tao, S. Ruan, G. Xie, X. Kong, L. Shen, F. Meng, C. Liu, X. Zhang, W. Dong, W. Chen, Role of tungsten oxide in inverted polymer solar cells, Appl. Phys. Lett. 94 (2009), 043311, https://doi.org/10.1063/1.3076134.
[21] Ç. Kırbıyık, S. Büyükçelebi, M.Z. Yiğit, M. Can, K. Kara, M. Kuş, D.A. Kara, Improving the performance of inverted polymer solar cells through modification of compact TiO_2 layer by different boronic acid functionalized self-assembled monolayers, Appl. Surf. Sci. 479 (2019) 177–184, https://doi.org/10.1016/j.apsusc.2019.01.268.
[22] P. Qin, Q. He, D. Ouyang, G. Fang, W.C.H. Choy, G. Li, Transition metal oxides as hole-transporting materials in organic semiconductor and hybrid perovskite based solar cells, Sci. China Chem. 60 (2017) 472–489, https://doi.org/10.1007/s11426-016-9023-5.
[23] I. Ullah, S.K. Shah, S. Wali, K. Hayat, S.A. Khattak, A. Khan, Enhanced efficiency of organic solar cells by using ZnO as an electron-transport layer, Mater. Res. Express 4 (2017), 125505, https://doi.org/10.1088/2053-1591/aa9dc9.
[24] H. Cheun, J.D. Berrigan, Y. Zhou, M. Fenoll, J. Shim, C. Fuentes-Hernandez, K. H. Sandhage, B. Kippelen, Roles of thermally-induced vertical phase segregation and crystallization on the photovoltaic performance of bulk heterojunction inverted polymer solar cells, Energy Environ. Sci. 4 (2011) 3456, https://doi.org/10.1039/c1ee01316e.
[25] J.-C. Wang, W.-T. Weng, M.-Y. Tsai, M.-K. Lee, S.-F. Horng, T.-P. Perng, C.-C. Kei, C.-C. Yu, H.-F. Meng, Highly efficient flexible inverted organic solar cells using atomic layer deposited ZnO as electron selective layer, J. Mater. Chem. 20 (2010) 862–866, https://doi.org/10.1039/B921396A.
[26] S. Chambon, L. Derue, M. Lahaye, B. Pavageau, L. Hirsch, G. Wantz, MoO_3 thickness, thermal annealing and solvent annealing effects on inverted and direct polymer photovoltaic solar cells, Materials (Basel) 5 (2012) 2521–2536, https://doi.org/10.3390/ma5122521.
[27] C. Tao, G. Xie, F. Meng, S. Ruan, W. Chen, Tailoring spatial distribution of the optical field intensity in semitransparent inverted organic solar cells, J. Phys. Chem. C 115 (2011) 12611–12615, https://doi.org/10.1021/jp201890q.
[28] R. Lampande, G.W. Kim, J. Boizot, Y.J. Kim, R. Pode, J.H. Kwon, A highly efficient transition metal oxide layer for hole extraction and transport in inverted polymer bulk heterojunction solar cells, J. Mater. Chem. A. 1 (2013) 6895, https://doi.org/10.1039/c3ta10863e.
[29] K. Zilberberg, S. Trost, J. Meyer, A. Kahn, A. Behrendt, D. Lützenkirchen-Hecht, R. Frahm, T. Riedl, Inverted organic solar cells with sol-gel processed high work-function vanadium oxide hole-extraction layers, Adv. Funct. Mater. 21 (2011) 4776–4783, https://doi.org/10.1002/adfm.201101402.
[30] G. Terán-Escobar, J. Pampel, J.M. Caicedo, M. Lira-Cantú, Low-temperature, solution-processed, layered V_2O_5 hydrate as the hole-transport layer for stable organic solar cells, Energy Environ. Sci. 6 (2013) 3088, https://doi.org/10.1039/c3ee42204f.
[31] Y. Jouane, S. Colis, G. Schmerber, P. Kern, A. Dinia, T. Heiser, Y.-A. Chapuis, Room temperature ZnO growth by rf magnetron sputtering on top of photoactive P3HT: PCBM for organic solar cells, J. Mater. Chem. 21 (2011) 1953–1958, https://doi.org/10.1039/C0JM02354J.
[32] H. Simchi, B.E. McCandless, T. Meng, W.N. Shafarman, Structural, optical, and surface properties of WO_3 thin films for solar cells, J. Alloys Compd. 617 (2014) 609–615, https://doi.org/10.1016/j.jallcom.2014.08.047.
[33] F. Güzelçimen, B. Tanören, Ç. Çetinkaya, M.D. Kaya, H.İ. Efkere, Y. Özen, D. Bingöl, M. Sirkeci, B. Kınacı, M.B. Ünlü, S. Özçelik, The effect of thickness on surface structure of rf sputtered TiO_2 thin films by XPS, SEM/EDS, AFM and SAM, Vacuum 182 (2020), 109766, https://doi.org/10.1016/j.vacuum.2020.109766.
[34] M.T. Greiner, Z.-H. Lu, Thin-film metal oxides in organic semiconductor devices: their electronic structures, work functions and interfaces, NPG Asia Mater. 5 (2013), https://doi.org/10.1038/am.2013.29 e55–e55.
[35] Y.-P. Zhao, G.-C. Wang, T.-M. Lu, G. Palasantzas, J.T.M. De Hosson, Surface-roughness effect on capacitance and leakage current of an insulating film, Phys. Rev. B 60 (1999) 9157–9164, https://doi.org/10.1103/PhysRevB.60.9157.
[36] H.M. R, M.K. Khalaf, A.N.A. Al-Gaffer, Multilayer coatings D/M/D for solar reflector applications prepared by DC magnetron sputtering, in: AIP Conf. Proc, 2020, 020311, https://doi.org/10.1063/5.0000449.
[37] C.-Y. Chen, T.-C. Wei, P.-H. Hsiao, C.-H. Hung, Vanadium oxide as transparent carrier-selective layer in silicon hybrid solar cells promoting photovoltaic performances, ACS Appl. Energy Mater. 2 (2019) 4873–4881, https://doi.org/10.1021/acsaem.9b00565.
[38] H. Ma, H. Fang, W. Wu, C. Zheng, L. Wu, H. Wang, A highly transparent humidity sensor with fast response speed based on α-MoO_3 thin films, RSC Adv. 10 (2020) 25467–25474, https://doi.org/10.1039/D0RA03958F.
[39] W.L. Kwong, N. Savvides, C.C. Sorrell, Electrodeposited nanostructured WO_3 thin films for photoelectrochemical applications, Electrochim. Acta 75 (2012) 371–380, https://doi.org/10.1016/j.electacta.2012.05.019.
[40] H. Essaidi, L. Cattin, Z. El Jouad, S. Touihri, M. Blais, E. Ortega, G. Louarn, M. Morsli, T. Abachi, T. Manoubi, M. Addou, M.A. del Valle, F. Diaz, J.C. Bernède, Indium free electrode, highly flexible, transparent and conductive for optoelectronic devices, Vacuum 153 (2018) 225–231, https://doi.org/10.1016/j.vacuum.2018.04.026.